

Performance Verification of $7,424 \times 7,424$ Optical Switch Offering $1.4 \mu\text{s}$ Switching Time

Ryosuke Matsumoto, Ryotaro Konoike, Hiroyuki Matsuura, Keijiro Suzuki,
Takashi Inoue, Kazuhiro Ikeda, Shu Namiki, and Ken-ichi Sato

National Institute of Advanced Industrial Science and Technology (AIST), 1-1-1 Umezono, Tsukuba, Ibaraki 305-8568, Japan
E-mail address: matsumoto.ryosuke@aist.go.jp

Abstract: We experimentally verify performance of $7,424 \times 7,424$ optical switches that offer $1.4\text{-}\mu\text{s}$ switching time. Two key enablers are reported; newly developed polarization-insensitive 64×1 silicon-photonic switches integrated with wavelength-tunable filters, and a fast burst-mode coherent receiver. © 2022 The Authors

1. Introduction

Reflecting the recent slow-down in Moore's law, optical switches are being introduced in data centers [1]. Presently 3D-MEMS optical switches are used to replace leaf switches (the uppermost tier switches). The available port count of 3D-MEMS optical switch is small (136×136 [1]) and hence a large number of optical switches must be used in parallel, which incurs complicated traffic engineering and optical switch multi-hops [1]. By increasing optical switch port count, network traffic engineering can be simplified and network throughput can also be enhanced (reduction of multi-hop optical connections). Furthermore, when the port count reaches several thousands, first-tier electrical switches (e.g., top-of-rack switches) can be directly connected via optical switches, eliminating all the higher-tier electrical switches. This yields significant electrical power reduction, simplified traffic engineering, reduced latency (eliminating queueing delay at multiple tiers of electrical switches traversed), and enhanced network bisection bandwidth that can reach 100 Pb/s [2]. Regarding the switching time requirement for optical switches, the hybrid switching scheme (retaining a small, say, 10–20% bandwidth electrical switching network in parallel) relaxes the time required to $\sim 10 \mu\text{s}$ and has been intensively investigated [2–5]. We have so far proposed large-scale and fast optical switch architectures combining wavelength and space division routing [6].

In this paper, we present a high-port-count and fast optical switch scalable to several thousands of ports, which is enabled by a newly developed silicon-photonic 64×1 space switch and burst-mode coherent receiver. The average switch loss is 9.4 dB which is attained by monolithically integrating a 64×1 selector switch and tunable filter (TF) with on-chip polarization diversity circuits. In the receiver, two-stage digital filters are cascaded to rapidly lock on burst signals: the first stage uses Stokes space for initial polarization estimation, while the second stage is based on the well-known constant-modulus algorithm (CMA). We verified the performances of the optical switch using 116-ch. \times 128-Gbps DP-QPSK signals; 7,424 port count and fast switching time of $1.4 \mu\text{s}$ were successfully realized.

2. High-port-count Optical Switch Architecture Employing Burst-mode Coherent Receivers

Figure 1 depicts our proposed $MN \times MN$ optical switch architecture utilizing a shared local oscillator (LO) bank for burst-mode coherent detection. The incident signals from N fixed-wavelength transmitters are aggregated by an $N \times 1$ multiplexer (MUX) and then distributed by a $1 \times (N/S)$ splitter. After loss compensation by EDFAs, the signals are further distributed by $1 \times S$ splitters. An $M \times M$ multicast switch (MCS) splits the input signals at a $1 \times M$ splitter and connects one of the M distributed signal groups with an $M \times 1$ selector. Some of N wavelengths in the selected signal are extracted by tunable filters (TF1s). Colorless detection allows removal of TF1 when the number of WDM channels is small. Finally, the filtered signal is coherently detected by using an LO sourced from the LO bank. In the LO bank, an optical comb source or N fixed-wavelength LDs aggregated with an $N \times 1$ MUX, and a cascade of a $1 \times (MN/S_L)$ splitter and $1 \times S_L$ splitters are used to broadcast the WDM channels. The target wavelength channel is then extracted by TF2 and amplified with a compact and low-cost preamplifier. The first ($1 \times MN/S_L$) splitter is followed by EDFAs; the output power is P_L dBm. The EDFAs in the optical switch or LO bank are shared by multiple output ports (S or S_L) to reduce cost. Consequently, a high-port-count and fast optical switch is cost-effectively built for

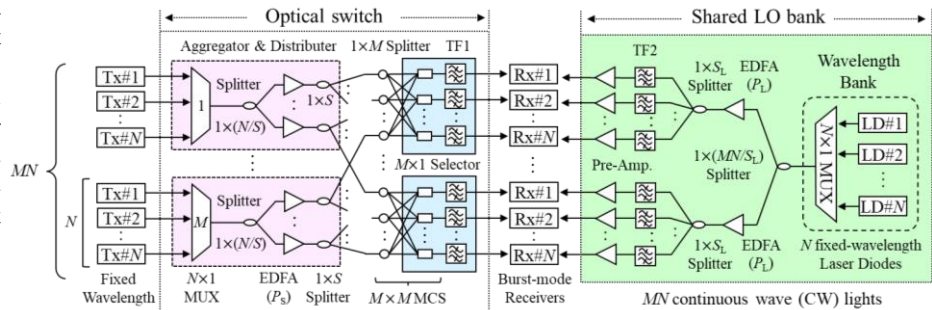


Fig. 1. $MN \times MN$ optical circuit switch architecture based on tunable filters for coherent detection.

Table 1. Achievable optical switch scale for each modulation format

| Modulation format (SC: Single carrier, DC: Dual carrier) | Channel speed [Gbps/ch.] | Number of wavelength (N) | Channel spacing [GHz] | $M = 64$ | |
|--|-----------------------------|------------------------------------|-----------------------------|----------------------|-----------------------------|
| | | | | Switch port count | Throughput [Tbps/switch] |
| 32Gbd SC DP-QPSK | 100 | 116 | 37.5 | 7,424 | 742.4 |
| 64Gbd SC DP-QPSK | 200 | 58 | 75 | 3,712 | 742.4 |
| 32Gbd DC DP-QPSK | | 88 | 50 | 5,632 | 1126.4 |
| 43Gbd SC DP-8QAM | 400 | 32 | 137.5 | 2,048 | 819.2 |
| 64Gbd DC DP-QPSK | | 48 | 100 | 3,072 | 1228.8 |
| 43Gbd DC DP-8QAM | | | | | |

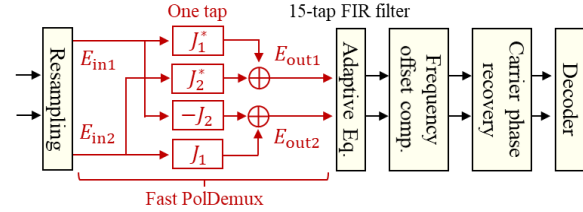


Fig. 2. Receiver DSP configuration for burst-mode reception.

coherent detection with LO wavelength filtering. Fast-converging digital signal processing (DSP) needs to be incorporated at the receiver for burst-mode operation, the detail of which is explained later.

We previously reported a $1,856 \times 1,856$ optical switch (combination of 32×32 space switches and 58 wavelengths) based on TFs [6]. The switch port count is given by MN . Larger space switches (M) incur larger loss. The available wavelength number (N) for colorless detection is limited by the receiver's specific dynamic range, 18 dB corresponds to ~ 63 channels ($= 10^{18/10}$) [7]. TF1 set in front of the receiver can mitigate receiver power saturation [8]. However, the extra component and additional loss are bothersome. To minimize these burdens, we developed a low-loss silicon-photonics $64(M) \times 1$ selector that is monolithically integrated with a TF, where we adopted TE-mode design and an on-chip polarization diversity scheme. This yielded a 64×64 MCS, and when using 116 wavelengths, a $7,424 \times 7,424$ optical switch was successfully developed as indicated in Table 1.

Figure 2 shows the configuration of our burst signal receiver DSP, its structure mirrors that used in the typical digital coherent receiver [9, 10], but employs fast polarization demultiplexing (PolDmux) prior to CMA-based adaptive equalization. The fast response of the DSP stems from the use of Stokes vector for polarization tracking [11, 12] and its adaptive operation without training sequences. Given the input electrical field vector $\mathbf{E}_{in} = [E_{in1}, E_{in2}]^T$ and tap coefficient vector $\mathbf{J} = [J_1, J_2]^T$ in Jones space, they are transformed into the Stokes vector $\mathbf{S} = [S_1, S_2, S_3]^T$ and $\mathbf{h} = [h_1, h_2, h_3]^T$, respectively. In the Stokes space, the k -th tap coefficient vector is updated at each symbol interval, following updating rule $\mathbf{h}(k) = \mathbf{h}(k-1) + \mu[\mathbf{S}(k) \cdot \mathbf{h}(k-1)]\mathbf{S}(k)$, where μ is the step-size parameter. This acts under Stokes space such that tap coefficient vector \mathbf{h} is perpendicular to input signal \mathbf{S} . After the conversion from the updated Stokes vector \mathbf{h} to Jones vector \mathbf{J} , the equalized outputs are given by $E_{out1} = J_1^* E_{in1} + J_2^* E_{in2}$ and $E_{out2} = -J_2^* E_{in1} + J_1^* E_{in2}$. Instantaneous convergence of the 1-tap butterfly finite impulse response (FIR) filter is achieved with the blind Stokes algorithm, by finding the normal vector of input symbol plane in three-dimensional Stokes space.

3. Prototype Fabrication of Polarization-Diversity 64×1 Silicon-Photonic Space Switch

We fabricated a polarization-insensitive and high-port-count space switch that integrates 64×1 selectors and TFs on a single silicon chip. It consisted of 126 symmetric Mach-Zehnder interferometer (MZI) element switches and 2 asymmetric MZI (AMZI) filters as illustrated in Fig. 3(a). To achieve polarization independency, two identical 64×1 selectors and TFs, which are designed for TE mode, are implemented on a polarization-diversity circuit using polarization splitter-rotators (PSRs). The space switch works for arbitrary input polarization as the PSR splits the two orthogonal polarizations and rotates TM light into TE light on the chip. Each 64×1 selector is configured by a six-stage cascade of 2×1 MZI element switches in a tree structure. The AMZI filter has the 3-dB bandwidth of ~ 19 nm, which is sufficient to prevent power saturation of receivers. All the MZIs are thermo-optically controlled by phase shifters. Figure 3(b) shows a micrograph of the fabricated chip with on-chip polarization diversity. The complete circuit fits in a footprint of 3×8 mm². Figure 3(c) depicts measured fiber-to-fiber insertion loss (F2F-IL) and polarization dependent loss (PDL) for all input ports at 1547 nm. The average IL over 64 input ports was 9.4 dB, and low average PDL of 0.27 dB was attained. The crosstalk was less than -20 dB over the C-band (35 nm).

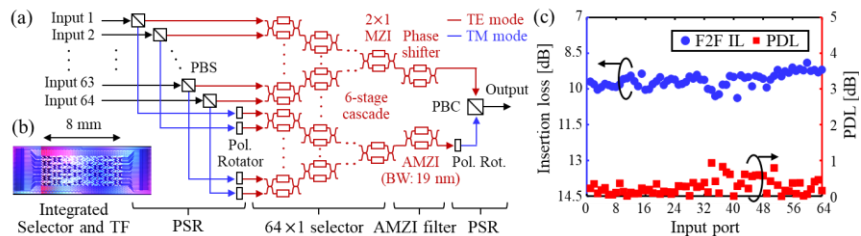


Fig. 3. Integrated polarization-insensitive 64×1 selector and tunable filter: (a) Structure. (b) Fabricated silicon-photonics chip. (c) Port dependency of insertion loss and PDL.

4. Experiments

Figure 4 shows the experimental setup of a $7,424 \times 7,424$ optical switch using the fabricated 64×1 space switch [Fig. 4(a)]. Seven channels, ranging from 1,530 nm to 1,565 nm with ~ 700 -GHz spacing, were bulk modulated using an IQ modulator (IQM) and arbitrary waveform generator (AWG). The generated signal was 32-Gbaud DP-QPSK shaped by a root-raised-cosine filter with a roll-off factor of 0.05. An overall 14.85-Tbps (116-ch. \times 128-Gbps DP-QPSK) WDM signal was assembled by combining a dummy channel [Fig. 4(b)], emulated by a spectrally-shaped amplified spontaneous emission (SS-ASE) light using a wavelength selective switch (WSS). The transmitted WDM signal was

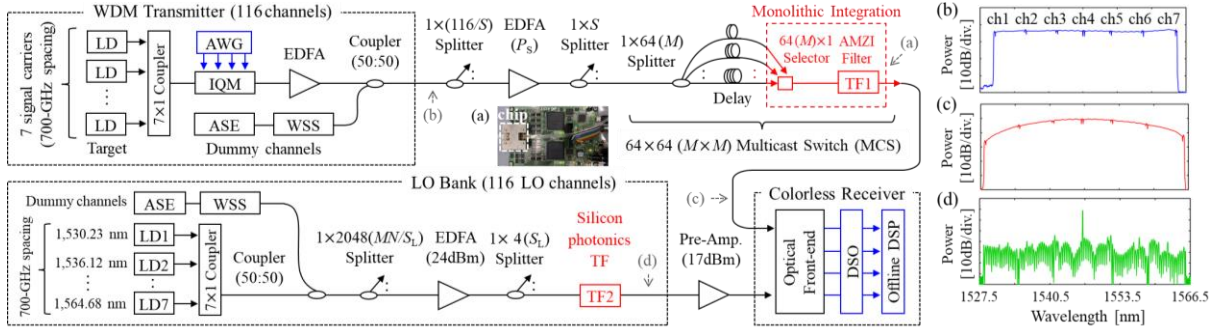


Fig. 4. Experimental setup of 7,424 × 7,424 optical switch with 32-Gbaud DP-QPSK signal ($M = 64$, $N = 116$, and $S_L = 4$). (a) Fabricated silicon-photonic 64×1 space switch mounted on printed circuit board with control electronics. Measured optical spectra after (b) WDM generation, (c) space switching through port 35, and (d) wavelength turning by silicon-photonic TF at 1547.116 nm (ch.4).

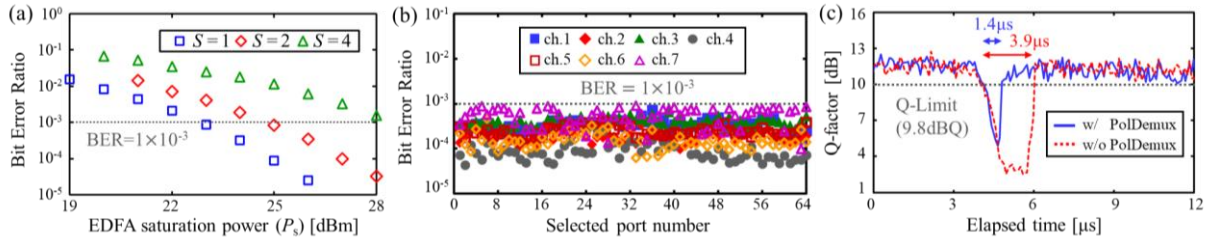


Fig. 5. Experimental results: (a) Measured BERs versus EDFA saturation power for different sharing number (S). (b) Measured BERs of all the combination of 7 channels and 64 space switch ports. (c) Q-factor transitions observed with and without fast PolDemux.

divided by a $1 \times (116/S)$ splitter, then amplified by an EDFA with saturation power of P_s , and further distributed by a $1 \times S$ splitter. In the 64×64 MCS, the incoming signals were broadcasted to 64 paths through 1×64 splitters and one path was selected using the fabricated module [Fig. 4(a)] that consisted of a 64×1 selector and TFs. To emulate crosstalk, the signals in the 64 paths were decorrelated by at least 100 symbols with fiber delay lines. Before the receiver, the TF1 makes the receiver properly work within the dynamic range [Fig. 4(c)]. In the LO bank, 37.5-GHz-spaced 116 LO channels were emulated by multiplexing seven LD lights with an SS-ASE light. The multiwavelength light was broadcasted using two-stage distributors ($1 \times 2,048$ and 1×4 splitters) and EDFAs to overcome the splitter losses. An identical wavelength channel to the target signal was extracted [Fig. 4(d)] by a recently fabricated silicon-photonic TF [13]. The target channel, amplified to 17 dBm via a burst-mode preamplifier, was used as an LO in the coherent receiver. The beat of the signal and LO was detected with an optical front-end, digitized using a digital storage oscilloscope (DSO). The detected signal was processed offline using the DSP of Fig. 2.

Figure 5(a) shows the dependency of EDFA sharing number (S), with the BERs selected through port 35 and measured on the central channel (ch.4; 1547.116 nm). For the EDFA saturation power (P_s), we found the value of 22.9 and 24.8 dBm yielded the BER of 1×10^{-3} for $S = 1$ and 2, respectively. Figure 5(b) shows measured signal quality variations with regard to channel frequency and space switch state. Successful switching of 448 channels ($7 \text{ WDM} \times 64$ ports) was confirmed with BERs below 1×10^{-3} . The switching performance was examined by simultaneously changing the optical path from port 1 to port 64 and the passband of the TFs from ch.3 to ch.4. Figure 5(c) displays the time-resolved Q-factor when the fast PolDemux was switched on and off. A short switching time of 1.4 μs was recorded with the burst-mode DSP, in contrast to the 3.9 μs achieved without the fast PolDemux.

5. Conclusions

By fabricating and testing a 64×1 space switch and burst-mode DSP that employs fast PolDemux, we demonstrated a 7,424 × 7,424 optical switch with the switching time of 1.4 μs . We envisage a 2.4-dB power budget improvement by reducing fiber-to-chip coupling loss from 2.6 dB/facet to 1.4 dB/facet as reported in our recent work [14].

Acknowledgement: A part of this paper is based on results obtained from the project JPNP16007 commissioned by the New Energy and Industrial Technology Development Organization (NEDO).

References

- [1] L. Poutievski et al., *Proc. ACM SIGCOMM*, p.66 (2022).
- [2] K. Sato, *Proc. ICCCN*, Invited Session 5, p. 1 (2021).
- [3] N. Farrington et al., *Proc. ACM SIGCOMM*, p.339 (2010).
- [4] G. Wang et al., *Proc. ACM SIGCOMM*, p.327 (2010).
- [5] N. Farrington et al., *Proc. OFC*, OW3H.3 (2013).
- [6] R. Matsumoto et al., *J. Lightw. Tech.*, **39**(8), p. 2263 (2021).
- [7] Optical Internetworking Forum (OIF), OIF-DPC-MRX-02.0.
- [8] Y. Mori et al., *J. Lightw. Tech.*, **38**(5), p.1002 (2020).
- [9] S. Savory, *Opt. Exp.*, **16**(2), p.804 (2008).
- [10] K. Kikuchi, *J. Lightw. Tech.*, **34**(1), p.157 (2015).
- [11] B. Szafraniec et al., *Opt. Exp.*, **18**(7), p.17928 (2010).
- [12] N. J. Muga et al., *J. Lightw. Tech.*, **32**(19), p.3290 (2014).
- [13] R. Matsumoto et al., *Proc. OFC*, M11.3 (2021).
- [14] K. Suzuki et al., *J. Lightw. Tech.*, **37**(1), p.116 (2019).